HHS Public Access

Author manuscript

Biochemistry. Author manuscript; available in PMC 2019 February 06.

Published in final edited form as:

Biochemistry. 2018 February 06; 57(5): 827–838. doi:10.1021/acs.biochem.7b01028.

Functional Contribution of the Spastic Paraplegia-Related Triglyceride Hydrolase DDHD2 to the Formation and Content of Lipid Droplets

Jordon M. Inloes[†], **William B. Kiosses**[‡], **Huajin Wang**[§,‖,⊥,#], **Tobias C. Walther**[⊥,#,@,▽], **Robert V. Farese Jr.**[⊥,#,@], and **Benjamin F. Cravatt**[*,†]

[†]Department of Chemical Physiology, The Skaggs Institute for Chemical Biology, The Scripps Research Institute, La Jolla, California 92037, United States

[‡]Department of Molecular Medicine, The Skaggs Institute for Chemical Biology, The Scripps Research Institute, La Jolla, California 92037, United States

[§]University Libraries, Carnegie Mellon University, Pittsburgh, Pennsylvania 15213, United States

[‖]Department of Biological Sciences, Carnegie Mellon University, Pittsburgh, Pennsylvania 15213, United States

[⊥]Department of Genetics and Complex Diseases, Harvard T. H. Chan School of Public Health, Boston, Massachusetts 02115, United States

[#]Department of Cell Biology, Harvard Medical School, Boston, Massachusetts 02115, United States

[@]Broad Institute of Harvard and MIT, Cambridge, Massachusetts 02142, United States

[▽]Howard Hughes Medical Institute, Boston, Massachusetts 02115, United States

Abstract

Deleterious mutations in the serine lipase DDHD2 are a causative basis of complex hereditary spastic paraplegia (HSP, subtype SPG54) in humans. We recently found that DDHD2 is a principal triglyceride hydrolase in the central nervous system (CNS) and that genetic deletion of this

[*]**Corresponding Author:** cravatt@scripps.edu.

Supporting Information

The Supporting Information is available free of charge on the ACS Publications website at DOI: 10.1021/acs.biochem.7b01028.
Supporting figures (Figures S1–S11), supplemental table (Table S1), and supplemental methods (PDF)
Spectral counts from four replicates of DDHD2$^{-/-}$ brain protein correlation profiling experiments (Table S2) (XLSX)
Lipid droplet-associated proteins and proteins with dual localization between the lipid droplet and other fractions derived by hierarchical clustering (Table S3) (XLSX) Peptide level data from four replicates of DDHD2$^{-/-}$ brain protein correlation profiling (Table S4) (XLSX)

ORCID

Benjamin F. Cravatt: 0000-0001-5330-3492

Author Contributions

J.M.I. and B.F.C. designed experiments, interpreted results, and wrote the paper. J.M.I. cloned DDHD2 mutants and performed lipid droplet accumulation experiments and lipid droplet proteomics. W.B.K. performed confocal microscopy data acquisition and analysis. H.W., T.C.W., and R.V.F. provided technical assistance with brain lipid droplet isolation.

Notes

The authors declare no competing financial interest.

enzyme in mice leads to ectopic lipid droplet (LD) accumulation in neurons throughout the brain. Nonetheless, how HSP-related mutations in DDHD2 relate to triglyceride metabolism and LD formation remains poorly understood. Here, we have characterized a set of HSP-related mutations in DDHD2 and found that they disrupt triglyceride hydrolase activity in vitro and impair the capacity of DDHD2 to protect cells from LD accumulation following exposure to free fatty acid, an outcome that was also observed with a DDHD2-selective inhibitor. We furthermore isolated and characterized LDs from brain tissue of DDHD2$^{-/-}$ mice, revealing that they contain both established LD-associated proteins identified previously in other organs and CNS-enriched proteins, including several proteins with genetic links to human neurological disease. These data, taken together, indicate that the genetic inactivation of DDHD2, as caused by HSP-associated mutations, substantially perturbs lipid homeostasis and the formation and content of LDs, underscoring the importance of triglyceride metabolism for normal CNS function and the key role that DDHD2 plays in this process.

Graphical abstract

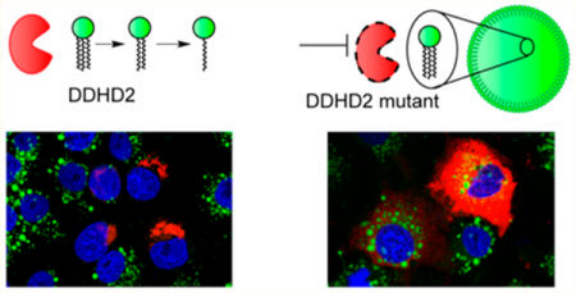

Exome sequencing has identified recessive, deleterious mutations in the *DDHD2* gene as a causative basis for complex hereditary spastic paraplegia (HSP).[1] HSP describes a set of genetically heterogeneous diseases related by common neurological phenotypes that include lower limb spasticity and weakness due to neurodegeneration of motor neurons, with complex forms of HSP also producing additional neurological symptoms.[2] The complex HSP subtype caused by *DDHD2* mutations is termed SPG54 and manifests as early-onset disease with spastic gait, intellectual disability, thin corpus callosum, and a lipid peak that can be detected in the brain by magnetic resonance spectroscopy.[1] Multiple *DDHD2* mutations have been linked to SPG54 that, despite representing different genetic variants (missense and frameshift) and being distributed throughout the protein-coding sequence of the gene, converge to produce similar neuropathologies.[3] One exception is a report of sisters with a homozygous V220F mutation in the DDHD2 protein that results in a distinct late-onset spastic ataxia syndrome.[4]

DDHD2 is part of a subgroup of serine hydrolases that includes the sequence-related proteins DDHD1 and SEC23IP.[5,6] Initial biochemical studies provided evidence that DDHD1 and DDHD2 can function as lipases,[6,7] hydrolyzing a range of (phospho)lipid substrates in vitro; nonetheless, the endogenous substrates and functions of these enzymes have remained poorly understood. We recently generated DDHD2$^{-/-}$ mice and found that these animals exhibited substantial elevations in the levels of triacylglycerols (TAGs) in the

central nervous system (CNS), which correlated with lipid droplet (LD) accumulation in neurons and cognitive and motor abnormalities that resemble complex HSP.[8] We confirmed that DDHD2 hydrolyzes TAGs and represents a substantial portion of the bulk TAG hydrolase activity of the mouse brain. This function appears to be primarily restricted to the CNS, as, in most peripheral tissues, PNPLA2 (or ATGL) serves as the principal TAG hydrolase.[9]

Having established that DDHD2 regulates TAG and LD content in the CNS, several important questions emerge. First, how do the HSP-associated mutations in DDHD2 affect the TAG hydrolase activity of this enzyme? Do these mutations also alter LD formation in cells that express DDHD2? Finally, do the LDs that accumulate in brain tissue from DDHD2$^{-/-}$ mice have unique protein and/or lipid content that might help to explain the biochemical basis for the neuropathologies caused by DDHD2 loss? Here, we address these questions using a combination of biochemical, cell biological, and proteomic methods. Specifically, we developed an in situ assay to measure the effect of DDHD2 and its HSP-related mutations on the accumulation of cellular TAGs and LDs, revealing that wild-type (WT) DDHD2, but not HSP mutant or chemically inhibited forms of this enzyme, suppresses LD formation in cells. We further purified LDs from brain tissue of DDHD2$^{-/-}$ mice and assessed their protein content by mass spectrometry-based proteomics, furnishing an inventory of proteins enriched in this subcellular compartment. The LD-enriched brain proteome included several proteins with established LD associations in peripheral tissues, as well as CNS-restricted proteins and proteins that are genetically linked to human neurological disease. Our proteomic analyses thus point to proteins and pathways that may be relevant to both HSP and a broader range of CNS disorders.

■ MATERIALS AND METHODS

Generation of DDHD2 Mutants

DDHD2 was amplified via polymerase chain reaction from human cDNA using the primers 5′-AAGCTTGCGGCCGCGATGTCATCAGTGCAGTCACAACAGG-3′ and 5′-ATCGATGGTACCGGTTACTGTAAAGGCTGATCAAGGAA-3′ and cloned into the NotI/KpnI site of pFLAG-CMV-6a (Sigma-Aldrich). HSP-associated DDHD2 mutations and an active-site S351A DDHD2 were generated by site-directed mutagenesis using mismatch-containing primers (Table S1). Mutagenesis was validated by Sanger sequencing. pFLAG-CMV-6a was modified to incorporate an N-terminal mCherry tag by amplifying mCherry using primers 5′-CGCGCGAAGCTTGTGAGCAAGGGCGAGGAGGA-3′ and 5′-AAGCAAGCGGCCGCCTTGTACAGCTCGTCCATGCC-3′ and cloned between HindIII/NotI sites to generate vector pFLAG-mCherry-CMV-6a. DDHD2 was subcloned from pFLAG-CMV-6a into pFLAG-mCherry-CMV-6a using NotI/KpnI sites.

Biochemical Studies

Recombinant expression of DDHD2, substrate assays, targeted lipid analysis, and activity-based protein profiling (ABPP) were performed using previously described methods[8] and are described in detail in the Supporting Information.

Oleic Acid-Induced Lipid Droplet Formation

Flag-tagged or mCherry-tagged constructs were transiently transfected in COS-7 cells and incubated for 24 h. For studies involving inhibitors, 2 μM KLH40 or KLH45 or dimethyl sulfoxide (DMSO) was added 1 h prior to oleic acid supplementation. Cells were supplemented with 10% (v/v) 2 mM oleic acid in 5% fatty acid free bovine serum albumin overnight without changing media. After 16 h in oleic acid-containing medium, cells were washed three times in PBS and either prepared for microscopy of lipidomic analysis.

Sample Preparation for Confocal Microscopy

Oleic acid-loaded cells were stained for fluorescence microscopy using previously published protocols.[10] Staining procedures were performed with cells adhered to glass coverslips in six-well tissue culture plates. Wash steps consisting of two washes with cold PBS were included between each step. Cells were fixed in 4% paraformaldehyde (Wako) for 20 min at room temperature and permeabilized with saponin (0.1 mg/mL) for 15 min at room temperature. BODIPY 493/503 (1 μg/mL) staining of lipid droplets was performed for 10 min at room temperature, followed by Hoecht 33342 (0.1 μg/mL) staining of nuclei for 30 min at room temperature. Slides were sealed with aqueous mounting medium (ProLong Gold, Life Technologies) and stored at 4°C.

Confocal Microscopy and Analysis

Samples on slides were prepared as described above and then imaged using a Zeiss 780 laser scanning confocal microscope. Three-dimensional eight-bit image stacks of the various fluorescent signals were acquired sequentially using a 63X (1.4 na) objective using a step size of 0.3 μm between images. These stacks of images were then projected into single stacks for two-dimensional analysis by using a maximum intensity projection macro in the Zeiss Zen software (Zeiss Inc., Thornwood, NY) or a similar macro in ImageJ (National Institutes of Health, Bethesda, MD). For further analysis of the fluorescent signals per cell, the images were imported into Image-Pro Premier software (Media Cybernetics, Rockville, MD). Here all labeled cells were autotraced using a region of interest module in the software based on their mCherry signal. These outlines were used to extract and/or score the total area and fluorescence signal of the BODIPY 493/503 signal within the autotraced cell outlines.[11] A defined threshold above background and autofluorescence was used for all BODIPY 493/503 relevant signal in the cells, and this range was 75–256 for the eight-bit images. These values of total BODIPY 493/503 signal per cell above background were then imported into Excel for further processing where we obtained integrated density values per cell (area × mean fluorescence intensity).

Sequential Fractionation of Mouse Brain Proteins

Brains from four DDHD2$^{-/-}$ mice were pooled and homogenized in 6 mL of homogenization buffer [200 mM sucrose, 20 mM Tris-HCl (pH 7.4), 1 mM EDTA, and Roche protease inhibitor] with 10 strokes of a dounce homogenizer. The homogenate was centrifuged (100000*g* for 1 h) in a SW 41 Ti swinging bucket rotor (Beckman) to pellet membranes. The supernatant was transferred to a clean 14 mL Thinwall Ultraclear tube (Beckman) for sucrose gradient fractionation. The pellet was probe sonicated in 3 mL of

homogenization buffer to resuspend, and a 1 mL aliquot was transferred to crush proof tubes. A series of differential centrifugation steps yielded insoluble fractions 7–9. Low-speed centrifugation (3000*g* for 30 min) generated a pellet that was saved as fraction 9. Moderate centrifugation (20000*g* for 30 min) generated a pellet that was saved as fraction 8. Ultracentrifugation (100000*g* for 1 h) pelleted microsomes that were saved as fraction 7.

The sucrose gradient was prepared by adjusting the density of the first 100000*g* supernatant with 1.5 volumes of 2 M sucrose in TBS. The supernatant was layered with 2 mL of 0.75 M sucrose in TBS, 0.5 M sucrose in TBS, and 0.25 M sucrose in TBS. The sucrose gradient was centrifuged (242000*g* for 3 h at 4°C) to separate lipid droplets from cytosolic proteins. The top fraction (0.5 mL) was collected with a tube slicer and saved as fraction 1. Subsequent 2 mL fractions were collected with a pipet and saved as fractions 2–6. Wessel–Flügge[12] protein precipitation was performed on all fractions, and proteins were solubilized in 4% sodium dodecyl sulfate. Protein concentrations were measured with the Pierce BCA assay kit.

Proteomic Sample Preparation

Mouse brain fractions were prepared for unenriched proteomics as described previously.[13] Protein from each fraction was denatured by adding 10 μM dithiothreitol and heating (30 min, 65°C), and then an aliquot equal to 5 μg of protein per fraction was diluted with 8 M urea and loaded onto a Microcon YM-30 filter unit. Tryptic peptides were collected in LoBind microcentrifuge tubes (Eppendorf) and acidified with formic acid [5% (v/v)].

Proteomics and Data Analysis

Mass spectrometry was performed with a Thermo Fisher LTQ Orbitrap Velos mass spectrometer coupled to an Agilent 1200 series quaternary pump following a previously published protocol.[14] Peptides were identified by the Integrated Proteomics Pipeline (IP2, Integrated Proteomics Applications, Inc. San Diego, CA. http://www.integratedproteomics.com) and grouped by UniProt protein ID. Spectral counts for each protein were compiled across 36 mass spectrometry runs and grouped by sucrose gradient fraction. Those proteins with at least 3 times as many spectral counts in fraction 1 versus the next most abundant fraction were designated LD-associated. Addition filtering criteria included detection in three of four fraction 1 replicates and having at least 15 spectral counts across all experiments. Additional details regarding chromatography, data searching, and clustering of proteomic experiments are included in the Supporting Information.

■ RESULTS

Functional Characterization of HSP-Associated Mutant Forms of DDHD2

DDHD2 is an ~80 kDa, multidomain serine hydrolase. Disease-causing mutations in DDHD2 occur throughout the protein sequence and are a mixture of missense, nonsense, and frameshift mutations.[1,3,4,15] Of these mutations, we generated nine DDHD2 mutants associated with HSP and one variant (V220F) associated with late-onset spastic ataxia (Figure 1A and Table S1). We also generated a catalytically inactive mutant of DDHD2 in

which the conserved serine nucleophile was mutated to alanine (S351A). WT and mutant forms of DDHD2 were expressed in HEK293T cells as N-terminal FLAG epitope-tagged proteins by transient transfection, and protein expression was assessed by anti-FLAG Western blotting (Figure 1B,C). Missense mutants (W103R, V220F, S351A, and D660H) displayed immunoreactivity at the expected parental molecular weight but showed some variation in intensity, with the D660H mutant, in particular, displaying a lower level of expression. As expected, most of the frameshift mutations and nonsense mutations generated DDHD2 variants of a smaller size that matched the predicted molecular weights of the truncated protein products. The expression level of these truncated proteins was also reduced compared to that of WT DDHD2, with four cases (R287*, I463H fs*6, R516*, and T602I fs*18) producing very small amounts of protein.

We next used the previously described activity-based protein profiling (ABPP) probe HT-01[16] to assess the activity of DDHD2 mutants. Among the 10 mutants, only two (W103R and V220F) displayed HT-01 reactivity (Figure 1D,E), with the former variant showing large reductions in the level of HT-01 labeling compared to that of WT DDHD2 [even when adjusted for protein quantity (Figure S1)]. The D660H, E686G fs35*, and Y661C fs*8 mutants, despite showing substantial expression in HEK293T cells, did not react with HT-01. We also performed TAG substrate hydrolysis assays with transfected HEK293T lysates[8] and found that only WT DDHD2 exhibited TAG hydrolysis activity greater than that observed in mock-transfected control cell lysates (Figure 1F). Finally, as expected, the S351A catalytic mutant did not show reactivity with HT-01 (Figure 1D,E) or TAG hydrolysis activity (Figure 1F), even though this variant displayed expression similar to that of WT DDHD2 (Figure 1B,C).

These results, taken together, indicate that HSP-associated mutations have a variable effect on the expression of DDHD2 but uniformly impair the catalytic activity of this enzyme.

WT DDHD2 Regulates TAG Storage in COS-7 Cells, but HSP-Associated Mutants Do Not

Genetic disruption of DDHD2 in mice leads to accumulation of intracellular lipid droplets (LDs) in neurons throughout the brain,[8] suggesting that DDHD2, presumably by acting as a TAG hydrolase, regulates LD formation and content. To test this hypothesis, we established a cell-based assay to monitor LD accumulation in COS-7 cells, which have served as a useful cell model for imaging LDs and LD-associated proteins.[17,18] COS-7 cells were transfected with mCherry fusion proteins of DDHD2 variants or the mCherry protein alone as a control. Cells were then treated with oleic acid [C18:1 free fatty acid (FFA), 200 μM] to promote the formation of LDs, and the BODIPY 493/503 dye[19] was used to image the LD content of cells expressing DDHD2 variants (Figure 2A).

Previous studies have suggested that DDHD2 localizes to the cis-Golgi and endoplasmic reticulum (ER)–Golgi intermediate compartment.[20] However, we found that WT DDHD2 showed a perinuclear subcellular distribution that was proximal to but largely nonoverlapping with the cis-Golgi apparatus (Figure S2). In reviewing past findings, we noted that original reports of DDHD2 subcellular localization also described a perinuclear distribution that only partly overlapped with cis-Golgi markers.[7] These data, taken together, indicate that WT DDHD2 localizes to a subcellular membrane compartment that is proximal

to but distinct from classical ER or cis-Golgi compartments. In contrast to the punctate, perinuclear localization of WT DDHD2, HSP-associated DDHD2 mutants (W103R, V220F, and Y661C fs*8) tended to display a more diffuse cellular profile (Figure 2A). WT DDHD2-transfected cells also exhibited decreased LD content compared to cells expressing HSP-associated DDHD2 mutants, the S351A mutant, or mCherry (Figure 2A and Figure S3), as quantified by measuring the LD surface area (Figure 2B) or BODIPY 493/ 503 dye intensity (Figure 2C) in transfected cells. Is it necessary to restate this observation?

We also found that oleic acid-loaded COS-7 cells expressing WT DDHD2, but not HSP-associated mutant forms of this protein (or the S351A mutant), displayed a lower TAG content and a correspondingly elevated diacylglycerol (DAG), monoacylglycerol (MAG), and free fatty acid (FFA) (Figure 3A–D and Figure S4) content compared to those of mCherry- expressing control cells. These data, combined with the LD measurements noted above, indicate that WT DDHD2 suppresses LD accumulation in fatty acid-loaded cells by hydrolyzing TAG, a key component of LDs, to generate the corresponding DAG, MAG, and FFA products. In contrast, the impaired TAG hydrolysis activity displayed by HSP-associated mutant forms of DDHD2 results in an inability to perturb LD formation in fatty acid-loaded cells.

We previously described a selective and in vivo-active inhibitor of DDHD2, KLH45, and a structurally related DDHD2-inactive control compound, KLH40.[8] We first confirmed inhibition of WT DDHD2 by treating transfected COS-7 cells with a concentration range of KLH45 (or KLH40) for 16 h, followed by ABPP with the DDHD2 probe HT-01 or the general serine hydrolase probe fluorophosphonate rhodamine (FP-Rh). This experiment revealed that KLH45, but not KLH40, selectively blocked DDHD2 activity, with complete inhibition being observed with 2 μM KLH45 (Figure S5). Treatment of WT DDHD2-transfected COS-7 cells with KLH45 (2 μM) prior to loading these cells with oleic acid (200 μM, 16 h) reversed the inhibitory effect of DDHD2 expression on LD accumulation (Figure 4A–C). In contrast, treatment of WT DDHD2-transfected COS-7 cells with the control compound KLH40 did not rectify the suppressed LD content of these cells. Consistent with these LD imaging results, we found that WT DDHD2-transfected COS-7 cells treated with DMSO or KLH40 showed lower TAG content and elevated quantities of the TAG hydrolysis products DAG, MAG, and FFA compared to those of WT DDHD2-transfected COS-7 cells treated with KLH45, which did not differ in their lipid profile from mCherry-transfected control cells (Figure 5A–C and Figure S6A–C).

These results, taken together, provide strong evidence that WT DDHD2, by acting as a TAG hydrolase, can regulate the LD content of mammalian cells, and this function is impaired by HSP-associated mutations or active-site-directed inhibitors of the enzyme.

Assessing the Protein Composition of LDs from DDHD2$^{-/-}$ Brain Tissue

LDs are cytoplasmic organelles composed of a neutral lipid core surrounded by a monolayer of phospholipids and can be enriched by tissues and cells based on their buoyant properties in a sucrose gradient.[21] Proteins are targeted to LDs by multiple mechanisms, including structural motifs, migration from the endoplasmic reticulum through LD bridges, and/or lipid post-translational modifications.[22–24] The protein composition of LDs has been

reported for a number of mammalian tissues and cells[25] but not, to the best of our knowledge, from brain tissue, where LDs are rare organelles, despite having several perceived functions in nervous system physiology and disease.[26,27]

Protein correlation profiling, a technique in which the relative quantities of proteins are estimated across fractionated proteomic samples, has proven to be a useful method for identifying proteins that are enriched in the LD fraction of cells and tissues.[28,29] We applied this method to DDHD2$^{-/-}$ brains, which were homogenized and sequentially fractionated by differential centrifugation and density gradient centrifugation, after which proteins in each fraction were precipitated and analyzed by liquid chromatography and tandem mass spectrometry on a Thermo Fisher LTQ Orbitrap Velos instrument, where the relative quantity of proteins across the fractions was estimated by spectral counting (Figure 6A and Table S2). In this experimental setup, LD-associated proteins should be enriched in the most buoyant fraction (fraction 1). We performed four biological replicates, and spectral count measurements were highly reproducible for proteins across replicate samples (Figure 6B; Pearson correlation coefficients R of >0.8; also see Figure S7). Similar experiments were attempted in DDHD2$^{+/+}$ brains, but fraction 1 from these samples contained only 10% of the total protein quantity found in fraction 1 from DDHD2$^{-/-}$ brains, consistent with the much more limited LD content of wild-type brain tissue.

A search of the normalized proteomic data revealed that marker proteins of the plasma membrane (ATP1A1), nucleus (HIST1H2B), mitochondria (VDAC2), and endoplasmic reticulum (ER) (CALR) were enriched in the heavier insoluble fractions 7–9, while the soluble cytosolic protein GAPDH was enriched in fractions 3–6 (Figure 6C and Table S2). ER-associated proteins also often had a second peak in fraction 2, which could correspond to the smooth ER component of brain tissue. Importantly, established LD proteins, such as PLIN2, were enriched in fraction 1 (Figure 6C and Table S2). We accordingly designated proteins as LD-associated if they showed their highest relative spectral count value in fraction 1 that was also at least 3 times greater in magnitude than that of the next highest fraction. We further required that, for a protein to be designated as LD-associated, it be observed in fraction 1 in at least three of the four biological replicates and assigned at least 15 total spectral counts across all experiments. Thirty-nine proteins satisfied the aforementioned criteria (Table 1), and a representative subset of correlation profiles for these proteins is shown in Figure 6D. Analysis of GO terms enriched in the LD-associated proteins returned lipid droplet (GO:0005811) as the most significantly overrepresented term (Figure S8), and several of these proteins (19 of 39) have also been linked to LDs in previous proteomic experiments with other mammalian cells and tissues (Table 1). A literature review of additional LD-associated proteins identified in DDHD2$^{-/-}$ brain tissue revealed that AGPAT6 and RDH10 have also been found to localize to LDs.[17,43] Sixteen remaining proteins represented novel candidate LD-associated proteins (Table 1), and a subset of these proteins were restricted in expression to the CNS (CBLN1, EPHX4, and VPS13C) (Figure S9). Detection of APOB as a LD-associated protein likely results from blood contamination in the preparation of the brain LD fraction. Several of the LD-associated proteins are associated with human neurological diseases, including GRN (frontotemporal dementia and neuronal ceroid lipofuscinosis), VPS13C (Parkinson's disease), and WDR45 (neurodegeneration with brain iron accumulation) (Table 1).

As a complement to the aforementioned filtering criteria for identifying LD-associated proteins, we analyzed the proteomic spectral count data using hierarchical means clustering, as described previously,[29] to group proteins that showed similar protein correlation profiles (Figure 6E). This analysis furnished a cluster of proteins primarily present in fraction 1 that contained all 39 proteins described above and an additional 10 proteins, including proteins involved in lipid metabolism, such as NSDHL and ACLS4 (Table S3). The clustering output also uncovered proteins with dual representation in fraction 1 (LDs) and other fractions (Figure S10 and Table S3). For instance, several proteins were found in both fractions 1 and 8 that corresponded to endosomal/lysosomal proteins (Figure S10), such as MAPK and MTOR activator 1 (LAMTOR1), cathepsin D (CTSD), and protein palmitoyl transferase 1 (PPT1). These results could indicate that, in DDHD2$^{-/-}$ brain tissue, a subset of LDs are fused to lysosomes, possibly to undergo degradation by a form of autophagy known as lipophagy.[44] Potentially consistent with this hypothesis, we also found proteins involved in autophagy processes, such as ATG2A, ATG2B, WDR45, and VPS13C, in the LD fraction (fraction 1). It is worth noting that ATG2A and ATG2B have been found to localize to LDs and influence their size and cellular distribution, suggesting a direct functional relationship between a subset of the autophagy network and LD structure and distribution.[38]

Finally, we also analyzed the lipid composition of LDs from brain tissue of DDHD2$^{-/-}$ mice. The hydrophobic core of LDs typically contains a mixture of TAGs and cholesterol esters that can vary in relative quantity depending on tissue type.[45] TLC analysis of lipid extracts from DDHD2$^{-/-}$ brain LDs revealed that they are primarily composed of TAGs and phospholipids with smaller quantities of cholesterol esters (Figure 7A,B).

These data, taken together, indicate that LDs originating from brain tissue of DDHD2$^{-/-}$ mice contain both shared and unique sets of proteins compared to LDs from other mammalian tissues and are enriched with TAGs, a principal substrate class of DDHD2.

■ DISCUSSION

Lipid droplets (LDs) in adipose tissue, liver, and muscle are used as storage depots for excess energy that can be liberated in response to energy demands.[47] In these tissues, the TAG hydrolase PNPLA2 plays a central role in regulating LD content.[9,48] The healthy brain, in contrast, has very few LDs, and the TAG composition of neurons is generally unaffected by genetic disruption of PNPLA2, which is not robustly expressed in brain tissue (Figure S11).[49] Recent studies indicate that DDHD2 serves as a principal TAG hydrolase in the nervous system, where the genetic disruption of this enzyme leads to ectopic deposition of LDs in neurons throughout the brain.[8] The fact that deleterious mutations in the human *DDHD2* gene also produce the neurological disorder complex hereditary spastic paraplegia (HSP) points to the regulation of LD content as a key factor in preserving neuronal physiology and function. Here, we sought to understand how HSP-associated mutations affected DDHD2 function using a combination of biochemical, chemical biology, and cell biology assays.

Our findings collectively support a model in which HSP-associated mutations impair the TAG hydrolase activity of DDHD2, which in turn disrupts the capacity of this enzyme to

limit LD formation in cells. Among the DDHD2 mutations, the V220F variant is atypical in that it causes a later onset disease termed hereditary spastic ataxia. We found that the protein expression and HT-01 reactivity of V220F DDHD2 were unperturbed, but the TAG hydrolase activity of this variant was markedly reduced compared to that of WT DDHD2. These data are consistent with reports that the V220F DDHD2 protein displays less activity with a phosphatidic acid (PA) substrate,[4] although some residual activity against this phospholipid substrate was observed. It is possible that the apparent disparity in activity displayed by V220F DDHD2 in experiments measuring HT-01 reactivity and TAG versus phospholipid turnover reflects differences in the dynamic range of these assays; however, V220F DDHD2 also showed impairments on par with other HSP-associated mutants in cellular assays of TAG and LD content. Thus, it is alternatively possible that the V220F DDHD2 mutant exhibits selective deficiency in TAG substrate recognition, although how this profile produces a less severe neurological disease outcome remains unknown. We also note that pathogenic mutations, including V220F, appear to alter the subcellular distribution of DDHD2 in transfected cells (Figure 2A), suggesting that mislocalization of these mutant proteins may also contribute to lipid droplet accumulation.

We also took advantage of the selective inhibitor KLH45 to confirm that acute pharmacological blockade of DDHD2 leads to TAG and LD accumulation in fatty acid-loaded cells. These experiments also provided a means of exploring whether WT DDHD2 localizes to LDs, a question that could not be addressed with the active enzyme because of its ability to prevent LD formation in fatty acid-loaded cells. In KLH45-treated cells, DDHD2 did not appear to bind directly to LDs but rather remained primarily associated with perinuclear membranes inhibitor treatment appears to also disrupt perinuclear localization of DDHD2 and so the ability of DDHD2 to associate with membranes may depend on enzyme activity (Figure 4A). In future studies, it would be interesting to examine how DDHD2 regulates LD content in cells without directly associating with this organelle. One possibility is that DDHD2 acts on nascent LDs (<200 nm diameter) that cannot readily be visualized by BODIPY 493/503 staining,[50] or perhaps DDHD2 consumes TAGs in other membrane organelles to limit the availability of these lipids for the formation of LDs.

Brain LDs, while rare in healthy individuals, are observed in a variety of neurodegenerative diseases, including Huntington's disease and Alzheimer's disease,[51,52] and SPG54 patients display a characteristic magnetic resonance spectroscopic peak reflecting lipid accumulation in the brain.[1,3] These findings point to a potential pathogenic role for LDs in the CNS, although our mechanistic understanding of this relationship remains limited. Determining the protein content of brain LDs represents an important first step toward elucidating LD functions in CNS physiology and disease. We accordingly took advantage of DDHD2$^{-/-}$ mice to characterize the proteomic content of LDs that accumulate in the brains of these animals. These studies confirmed the presence of several proteins that have been previously found to associate with LDs in other tissue and cell types, indicating a common set of proteins that bind to LDs from different origins. More interesting, however, was a subset of LD-associated proteins in DDHD2$^{-/-}$ brains that represent CNS-enriched proteins and proteins with direct genetic links to human neurological disease (Table 1). The distribution of these CNS-related proteins to LDs could alter their function, providing a potential mechanism by which LD accumulation in neurons promotes HSP and other neurological

disorders. The identification and characterization of proteins that promote LD formation in the CNS could accordingly reveal therapeutic targets for the treatment of neurological disease.

Supplementary Material

Refer to Web version on PubMed Central for supplementary material.

Acknowledgments

The authors are grateful to B. Kok, A. Galmozzi, and E. Saez [Saez laboratory, The Scripps Research Institute (TSRI)] for helpful discussions. The authors also thank L. Bar-Peled for confocal microscopy assistance (Cravatt laboratory, TSRI) and K. Lum and R. Suciu (Cravatt laboratory, TSRI) for helpful discussions and assistance with proteomic analysis. The animal experiments in this study were approved by the Scripps Research Institute Institutional Animal Care and Use Committee (IACUC 09-0041-03).

Funding

This work was supported by a Spastic Paraplegia Foundation grant (J.M.I.) and National Institutes of Health Grants R01 DA033760 (B.F.C.) and R01 GM097194 (T.C.W.).

References

1. Schuurs-Hoeijmakers JHM, Geraghty MT, Kamsteeg EJ, Ben-Salem S, de Bot ST, Nijhof B, van de Vondervoort GM II, van der Graaf M, Nobau AC, Otte-Höller I, Vermeer S, Smith AC, Humphreys P, Schwartzentruber J, FORGE Canada Consortium. Ali BR, Al-Yahyaee SA, Tariq S, Pramathan T, Bayoumi R, Kremer HPH, van de Warrenburg BP, van den Akker WMR, Gilissen C, Veltman JA, Janssen IM, Vulto-van Silfhout AT, van der Velde-Visser S, Lefeber DJ, Diekstra A, Erasmus CE, Willemsen MA, Vissers LELM, Lammens M, van Bokhoven H, Brunner HG, Wevers RA, Schenck A, Al-Gazali L, de Vries BBA, de Brouwer APM. Mutations in DDHD2, encoding an intracellular phospholipase A(1), cause a recessive form of complex hereditary spastic paraplegia. Am J Hum Genet. 2012; 91:1073–1081. [PubMed: 23176823]
2. Lo Giudice T, Lombardi F, Santorelli FM, Kawarai T, Orlacchio A. Hereditary spastic paraplegia: clinical-genetic characteristics and evolving molecular mechanisms. Exp Neurol. 2014; 261:518–539. [PubMed: 24954637]
3. Gonzalez M, Nampoothiri S, Kornblum C, Oteyza AC, Walter J, Konidari I, Hulme W, Speziani F, Schols L, Zuchner S, Schule R. Mutations in phospholipase DDHD2 cause autosomal recessive hereditary spastic paraplegia (SPG54). Eur J Hum Genet. 2013; 21:1214–1218. [PubMed: 23486545]
4. Doi H, Ushiyama M, Baba T, Tani K, Shiina M, Ogata K, Miyatake S, Fukuda-Yuzawa Y, Tsuji S, Nakashima M, Tsurusaki Y, Miyake N, Saitsu H, Ikeda SI, Tanaka F, Matsumoto N, Yoshida K. Late-onset spastic ataxia phenotype in a patient with a homozygous DDHD2 mutation. Sci Rep. 2015; 4:7132.
5. Tani K, Mizoguchi T, Iwamatsu A, Hatsuzawa K, Tagaya M. p125 is a novel mammalian Sec23p-interacting protein with structural similarity to phospholipid-modifying proteins. J Biol Chem. 1999; 274:20505–20512. [PubMed: 10400679]
6. Higgs HN, Han MH, Johnson GE, Glomset JA. Cloning of a phosphatidic acid-preferring phospholipase A1 from bovine testis. J Biol Chem. 1998; 273:5468–5477. [PubMed: 9488669]
7. Nakajima KI, Sonoda H, Mizoguchi T, Aoki J, Arai H, Nagahama M, Tagaya M, Tani K. A novel phospholipase A1 with sequence homology to a mammalian Sec23p-interacting protein, p125. J Biol Chem. 2002; 277:11329–11335. [PubMed: 11788596]
8. Inloes JM, Hsu KL, Dix MM, Viader A, Masuda K, Takei T, Wood MR, Cravatt BF. The hereditary spastic paraplegia-related enzyme DDHD2 is a principal brain triglyceride lipase. Proc Natl Acad Sci USA. 2014; 111:14924–14929. [PubMed: 25267624]

9. Haemmerle G, Lass A, Zimmermann R, Gorkiewicz G, Meyer C, Rozman J, Heldmaier G, Maier R, Theussl C, Eder S, Kratky D, Wagner EF, Klingenspor M, Hoefler G, Zechner R. Defective lipolysis and altered energy metabolism in mice lacking adipose triglyceride lipase. Science. 2006; 312:734–737. [PubMed: 16675698]
10. Listenberger, LL., Brown, DA. Current Protocols in Cell Biology. Wiley; New York: 2007. Fluorescent detection of lipid droplets and associated proteins. Chapter 24, Unit 24.2.11
11. Carames B, Kiosses WB, Akasaki Y, Brinson DC, Eap W, Koziol J, Lotz MK. Glucosamine activates autophagy in vitro and in vivo. Arthritis Rheum. 2013; 65:1843–1852. [PubMed: 23606170]
12. Wessel D, Flügge UI. A method for the quantitative recovery of protein in dilute solution in the presence of detergents and lipids. Anal Biochem. 1984; 138:141–143. [PubMed: 6731838]
13. Wisniewski JR, Zougman A, Nagaraj N, Mann M. Universal sample preparation method for proteome analysis. Nat Methods. 2009; 6:359–362. [PubMed: 19377485]
14. Martin BR, Wang C, Adibekian A, Tully SE, Cravatt BF. Global profiling of dynamic protein palmitoylation. Nat Methods. 2011; 9:84–89. [PubMed: 22056678]
15. Magariello A, Citrigno L, Zuchner S, Gonzalez M, Patitucci A, Sofia V, Conforti FL, Pappalardo I, Mazzei R, Ungaro C, Zappia M, Muglia M. Further evidence that DDHD2 gene mutations cause autosomal recessive hereditary spastic paraplegia with thin corpus callosum. Eur J Neurol. 2014; 21:e25–6. [PubMed: 24517879]
16. Hsu KL, Tsuboi K, Adibekian A, Pugh H, Masuda K, Cravatt BF. DAGLβ inhibition perturbs a lipid network involved in macrophage inflammatory responses. Nat Chem Biol. 2012; 8:999–1007. [PubMed: 23103940]
17. Wilfling F, Wang H, Haas JT, Krahmer N, Gould TJ, Uchida A, Cheng JX, Graham M, Christiano R, Fröhlich F, Liu X, Buhman KK, Coleman RA, Bewersdorf J, Farese RV, Walther TC. Triacylglycerol synthesis enzymes mediate lipid droplet growth by relocalizing from the ER to lipid droplets. Dev Cell. 2013; 24:384–399. [PubMed: 23415954]
18. Xu N, Zhang SO, Cole RA, McKinney SA, Guo F, Haas JT, Bobba S, Farese RV, Mak HY. The FATP1-DGAT2 complex facilitates lipid droplet expansion at the ER-lipid droplet interface. J Cell Biol. 2012; 198:895–911. [PubMed: 22927462]
19. Listenberger LL, Han X, Lewis SE, Cases S, Farese RV, Ory DS, Schaffer JE. Triglyceride accumulation protects against fatty acid-induced lipotoxicity. Proc Natl Acad Sci U S A. 2003; 100:3077–3082. [PubMed: 12629214]
20. Inoue H, Baba T, Sato S, Ohtsuki R, Takemori A, Watanabe T, Tagaya M, Tani K. Roles of SAM and DDHD domains in mammalian intracellular phospholipase A1 KIAA0725p. Biochim Biophys Acta, Mol Cell Res. 2012; 1823:930–939.
21. Ding Y, Zhang S, Yang L, Na H, Zhang P, Zhang H, Wang Y, Chen Y, Yu J, Huo C, Xu S, Garaiova M, Cong Y, Liu P. Isolating lipid droplets from multiple species. Nat Protoc. 2013; 8:43–51. [PubMed: 23222457]
22. Kory N, Farese RV, Walther TC. Targeting Fat: Mechanisms of Protein Localization to Lipid Droplets. Trends Cell Biol. 2016; 26:535–546. [PubMed: 26995697]
23. Zehmer JK, Bartz R, Bisel B, Liu P, Seemann J, Anderson RGW. Targeting sequences of UBXD8 and AAM-B reveal that the ER has a direct role in the emergence and regression of lipid droplets. J Cell Sci. 2009; 122:3694–3702. [PubMed: 19773358]
24. Wilfling F, Thiam AR, Olarte MJ, Wang J, Beck R, Gould TJ, Allgeyer ES, Pincet F, Bewersdorf J, Farese RV, Walther TC, Malhotra V. Arf1/COPI machinery acts directly on lipid droplets and enables their connection to the ER for protein targeting. eLife. 2014; 3:e01607. [PubMed: 24497546]
25. Yang L, Ding Y, Chen Y, Zhang S, Huo C, Wang Y, Yu J, Zhang P, Na H, Zhang H, Ma Y, Liu P. The proteomics of lipid droplets: structure, dynamics, and functions of the organelle conserved from bacteria to humans. J Lipid Res. 2012; 53:1245–1253. [PubMed: 22534641]
26. Welte MA. Expanding roles for lipid droplets. Curr Biol. 2015; 25:R470–81. [PubMed: 26035793]
27. Welte MA. How Brain Fat Conquers Stress. Cell. 2015; 163:269–270. [PubMed: 26451474]
28. Currie E, Guo X, Christiano R, Chitraju C, Kory N, Harrison K, Haas J, Walther TC, Farese RV. High confidence proteomic analysis of yeast LDs identifies additional droplet proteins and reveals

connections to dolichol synthesis and sterol acetylation. J Lipid Res. 2014; 55:1465–1477. [PubMed: 24868093]

29. Krahmer N, Hilger M, Kory N, Wilfling F, Stoehr G, Mann M, Farese RV, Walther TC. Protein correlation profiles identify lipid droplet proteins with high confidence. Mol Cell Proteomics. 2013; 12:1115–1126. [PubMed: 23319140]
30. Bartz R, Zehmer JK, Zhu M, Chen Y, Serrero G, Zhao Y, Liu P. Dynamic Activity of Lipid Droplets: Protein Phosphorylation and GTP-Mediated Protein Translocation. J Proteome Res. 2007; 6:3256–3265. [PubMed: 17608402]
31. Larsson S, Resjö S, Gomez MF, James P, Holm C. Characterization of the Lipid Droplet Proteome of a Clonal Insulin-producing β-Cell Line (INS-1 832/13). J Proteome Res. 2012; 11:1264–1273. [PubMed: 22268682]
32. Wan HC, Melo RCN, Jin Z, Dvorak AM, Weller PF. Roles and origins of leukocyte lipid bodies: proteomic and ultrastructural studies. FASEB J. 2007; 21:167–178. [PubMed: 17135363]
33. Umlauf E, Csaszar E, Moertelmaier M, Schuetz GJ, Parton RG, Prohaska R. Association of Stomatin with Lipid Bodies. J Biol Chem. 2004; 279:23699–23709. [PubMed: 15024010]
34. Orban T, Palczewska G, Palczewski K. Retinyl Ester Storage Particles (Retinosomes) from the Retinal Pigmented Epithelium Resemble Lipid Droplets in Other Tissues. J Biol Chem. 2011; 286:17248–17258. [PubMed: 21454509]
35. Kim SC, Chen Y, Mirza S, Xu Y, Lee J, Liu P, Zhao Y. A Clean, More Efficient Method for In-Solution Digestion of Protein Mixtures without Detergent or Urea. J Proteome Res. 2006; 5:3446–3452. [PubMed: 17137347]
36. Sato S, Fukasawa M, Yamakawa Y, Natsume T, Suzuki T, Shoji I, Aizaki H, Miyamura T, Nishijima M. Proteomic Profiling of Lipid Droplet Proteins in Hepatoma Cell Lines Expressing Hepatitis C Virus Core Protein. J Biochem. 2006; 139:921–930. [PubMed: 16751600]
37. Fujimoto Y, Itabe H, Sakai J, Makita M, Noda J, Mori M, Higashi Y, Kojima S, Takano T. Identification of major proteins in the lipid droplet-enriched fraction isolated from the human hepatocyte cell line HuH7. Biochim Biophys Acta, Mol Cell Res. 2004; 1644:47–59.
38. Velikkakath AKG, Nishimura T, Oita E, Ishihara N, Mizushima N. Mammalian Atg2 proteins are essential for autophagosome formation and important for regulation of size and distribution of lipid droplets. Mol Biol Cell. 2012; 23:896–909. [PubMed: 22219374]
39. Liu P, Ying Y, Zhao Y, Mundy DI, Zhu M, Anderson RGW. Chinese Hamster Ovary K2 Cell Lipid Droplets Appear to Be Metabolic Organelles Involved in Membrane Traffic. J Biol Chem. 2004; 279:3787–3792. [PubMed: 14597625]
40. Turró S, Ingelmo-Torres M, Estanyol JM, Tebar F, Fernández MA, Albor CV, Gaus K, Grewal T, Enrich C, Pol A. Identification and Characterization of Associated with Lipid Droplet Protein 1: A Novel Membrane-Associated Protein That Resides on Hepatic Lipid Droplets. Traffic. 2006; 7:1254–1269. [PubMed: 17004324]
41. Zehmer JK, Bartz R, Liu P, Anderson RGW. Identification of a novel N-terminal hydrophobic sequence that targets proteins to lipid droplets. J Cell Sci. 2008; 121:1852–1860. [PubMed: 18477614]
42. Wolins NE, Skinner JR, Schoenfish MJ, Tzekov A, Bensch KG, Bickel PE. Adipocyte protein S312 coats nascent lipid droplets. J Biol Chem. 2003; 278:37713–37721. [PubMed: 12840023]
43. Jiang W, Napoli JL. The retinol dehydrogenase Rdh10 localizes to lipid droplets during acyl ester biosynthesis. J Biol Chem. 2013; 288:589–597. [PubMed: 23155051]
44. Singh R, Kaushik S, Wang Y, Xiang Y, Novak I, Komatsu M, Tanaka K, Cuervo AM, Czaja MJ. Autophagy regulates lipid metabolism. Nature. 2009; 458:1131–1135. [PubMed: 19339967]
45. Walther TC, Farese RV. Lipid droplets and cellular lipid metabolism. Annu Rev Biochem. 2012; 81:687–714. [PubMed: 22524315]
46. Harris CA, Haas JT, Streeper RS, Stone SJ, Kumari M, Yang K, Han X, Brownell N, Gross RW, Zechner R, Farese RV. DGAT enzymes are required for triacylglycerol synthesis and lipid droplets in adipocytes. J Lipid Res. 2011; 52:657–667. [PubMed: 21317108]
47. Farese RV, Walther TC. Lipid droplets finally get a little R-E-S-P-E-C-T. Cell. 2009; 139:855–860. [PubMed: 19945371]

48. Haemmerle G, Moustafa T, Woelkart G, Büttner S, Schmidt A, van de Weijer T, Hesselink M, Jaeger D, Kienesberger PC, Zierler K, Schreiber R, Eichmann T, Kolb D, Kotzbeck P, Schweiger M, Kumari M, Eder S, Schoiswohl G, Wongsiriroj N, Pollak NM, Radner FPW, Preiss-Landl K, Kolbe T, Rülicke T, Pieske B, Trauner M, Lass A, Zimmermann R, Hoefler G, Cinti S, Kershaw EE, Schrauwen P, Madeo F, Mayer B, Zechner R. ATGL-mediated fat catabolism regulates cardiac mitochondrial function via PPAR-α and PGC-1. Nat Med. 2011; 17:1076–1085. [PubMed: 21857651]

49. Etschmaier K, Becker T, Eichmann TO, Schweinzer C, Scholler M, Tam-Amersdorfer C, Poeckl M, Schuligoi R, Kober A, Chirackal Manavalan AP, Rechberger GN, Streith IE, Zechner R, Zimmermann R, Panzenboeck U. Adipose triglyceride lipase affects triacylglycerol metabolism at brain barriers. J Neurochem. 2011; 119:1016–1028. [PubMed: 21951135]

50. Wang H, Becuwe M, Housden BE, Chitraju C, Porras AJ, Graham MM, Liu XN, Thiam AR, Savage DB, Agarwal AK, Garg A, Olarte MJ, Lin Q, Fröhlich F, Hannibal-Bach HK, Upadhyayula S, Perrimon N, Kirchhausen T, Ejsing CS, Walther TC, Farese RV. Seipin is required for converting nascent to mature lipid droplets. eLife. 2016; 5:440.

51. Yang DS, Stavrides P, Saito M, Kumar A, Rodriguez-Navarro JA, Pawlik M, Huo C, Walkley SU, Saito M, Cuervo AM, Nixon RA. Defective macroautophagic turnover of brain lipids in the TgCRND8 Alzheimer mouse model: prevention by correcting lysosomal proteolytic deficits. Brain. 2014; 137:3300–3318. [PubMed: 25270989]

52. Martinez-Vicente M, Talloczy Z, Wong E, Tang G, Koga H, Kaushik S, de Vries R, Arias E, Harris S, Sulzer D, Cuervo AM. Cargo recognition failure is responsible for inefficient autophagy in Huntington's disease. Nat Neurosci. 2010; 13:567–576. [PubMed: 20383138]

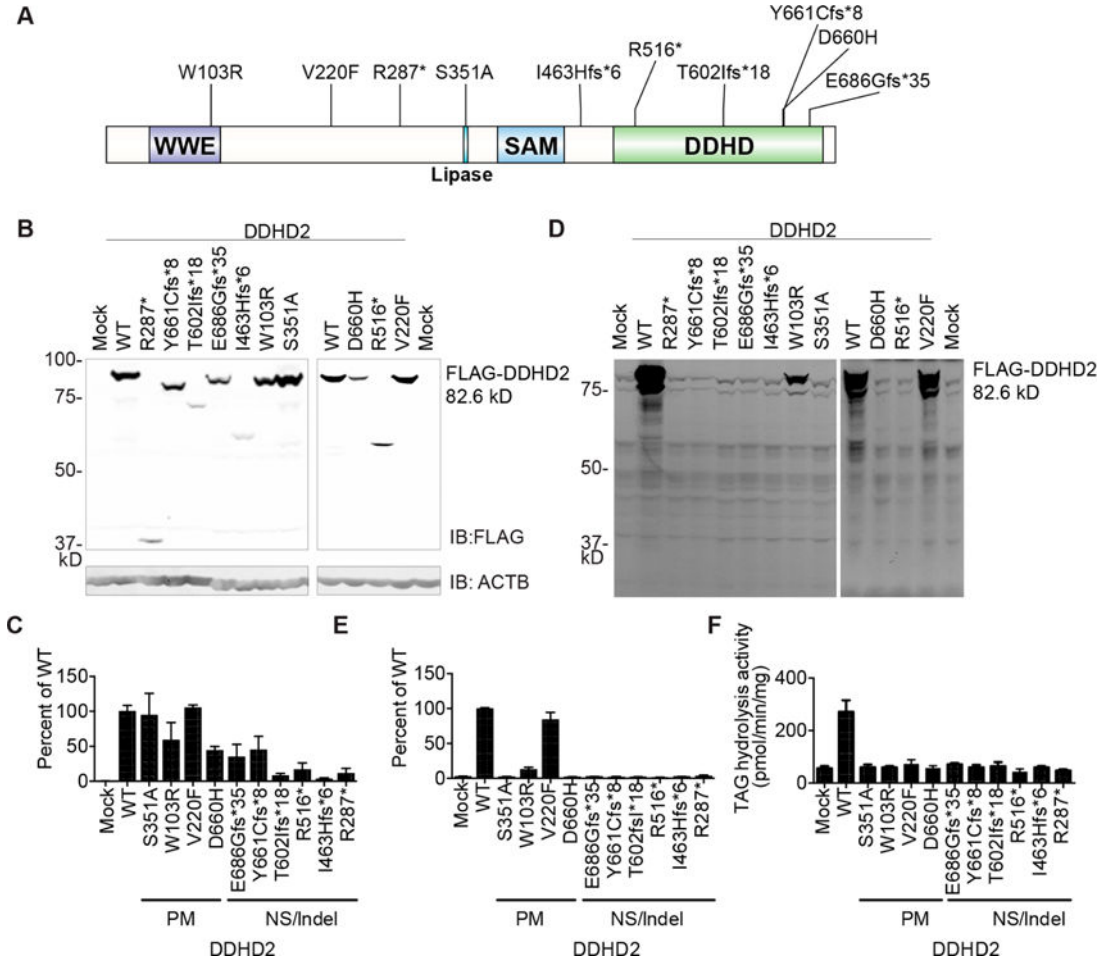

Figure 1.

HSP-associated mutations affect the expression and catalytic activity of DDHD2. (A) Domain diagram of human DDHD2 protein with locations of HSP-associated and catalytic (S351A) mutations indicated above the domain map bar. (B) Representative anti-FLAG immunoblots of lysates from HEK293T cells transfected with the indicated N-terminal FLAG-DDHD2 constructs. Note that frameshift and nonsense mutants result in bands of lower molecular weight that generally match the predicted sizes of truncated products from the DDHD2 sequence. (C) Quantification of anti-FLAG immunoblotting signals in panel B. Data represent average values ± the standard error of the mean (SEM) ($N = 4$ biological replicates). (D) ABPP of lysates from HEK293T cells transfected with the indicated N-terminal FLAG-DDHD2 constructs using the DDHD2-directed probe HT-01 (1 μM, 30 min). HT-01-treated samples were analyzed by sodium dodecyl sulfate—polyacrylamide gel electrophoresis and in-gel fluorescence scanning (fluorescent gel shown in grayscale). (E) Quantification of HT-01 labeling from panel D. Data represent average values ± SEM ($N = 4$ biological replicates). (F) TAG hydrolysis activity of soluble lysates from HEK293T cells transfected with the indicated N-terminal FLAG-DDHD2 constructs. C18:1/C18:1/C18:1 TAG (167 μM) was used as a substrate, and the production of C18:1 FFA was measured by liquid chromatography and mass spectrometry. Data represent average values ± SEM ($N = 4$ biological replicates). For panels A—F, DDHD2 mutants are represented using the single-

letter amino acid abbreviation of the affected position. Mutations that result in a stop codon are denoted by*. The number following fs* represents the number of amino acids after a frameshift mutation until the first stop codon.

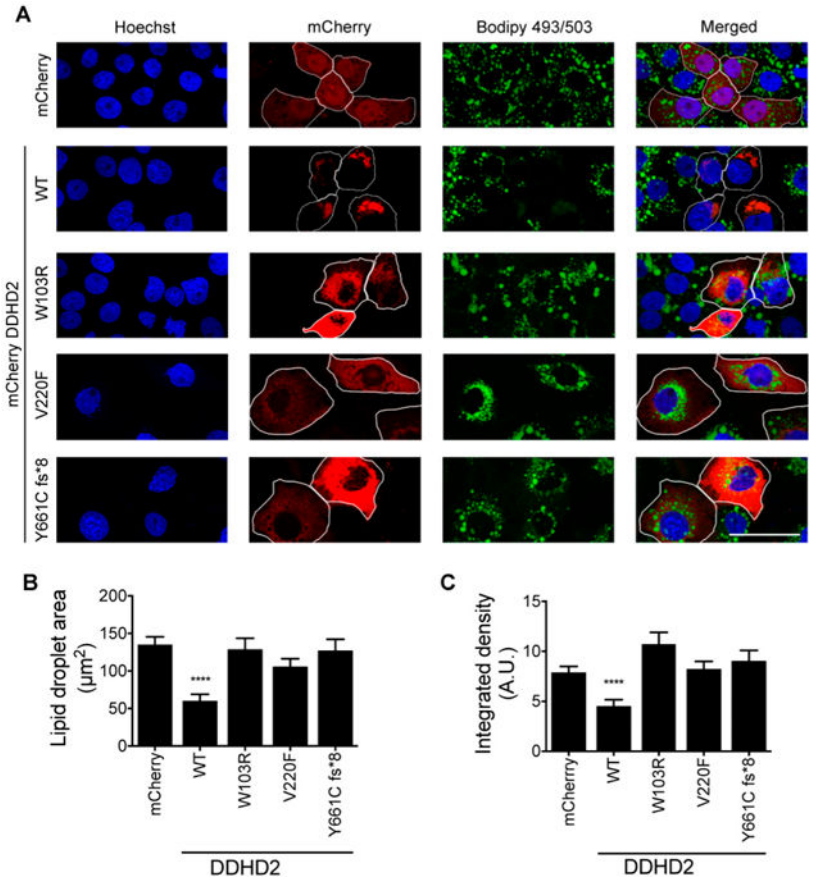

Figure 2.

DDHD2 expression suppresses the lipid droplet (LD) content of fatty acid-supplemented COS-7 cells. (A) COS-7 cells transfected with mCherry-DDHD2 variants or the mCherry control were loaded with C18:1 FFA overnight, and lipid droplets were imaged with the lipophilic dye BODIPY 493/503. Nuclei were stained with Hoechst. White outlines denote representative transfected cells as determined by mCherry signals. The scale bar is 50 μm. (B) Quantification of LD surface area per cell in COS-7 cells transfected with the indicated mCherry-DDHD2 constructs. (C) BODIPY 493/503 signal intensity per cell in COS-7 cells transfected with the indicated mCherry-DDHD2 constructs. Data represent average values ± SEM of 58–155 cells per group, and results are combined from at least two independent experiments. $^{****}P < 0.0001$ for DDHD2 variant-versus mCherry-transfected cells.

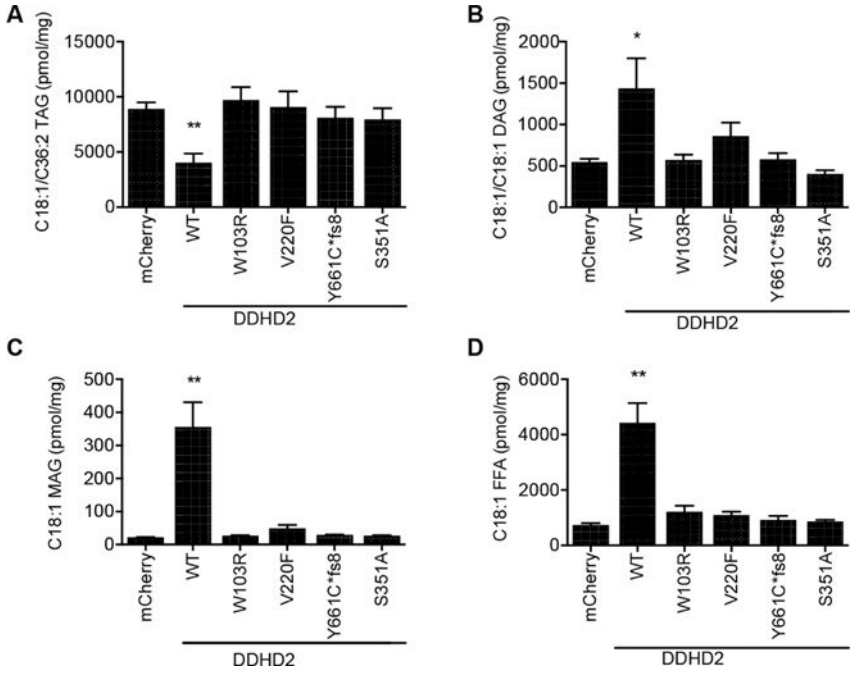

Figure 3.

WT DDHD2 alters TAG metabolism in fatty acid-supplemented COS-7 cells, but HSP-associated DDHD2 mutants do not. (A) The level of 18:1/36:2 TAG, the most abundant detected TAG species after oleic acid supplementation, is decreased in COS-7 cells relative to that in cells expressing mCherry and DDHD2 mutants. (B–D) Levels of 18:1/18:1 DAG, 18:1 MAG, and 18:1 FFA, respectively, are elevated in oleic acid-supplemented COS-7 cells expressing WT DDHD2 relative to cells expressing mCherry and DDHD2 mutants. Data represent means ± SEM (N=6 biological replicates). *P < 0.05 and **P < 0.01 for DDHD2- vs mCherry-transfected cells.

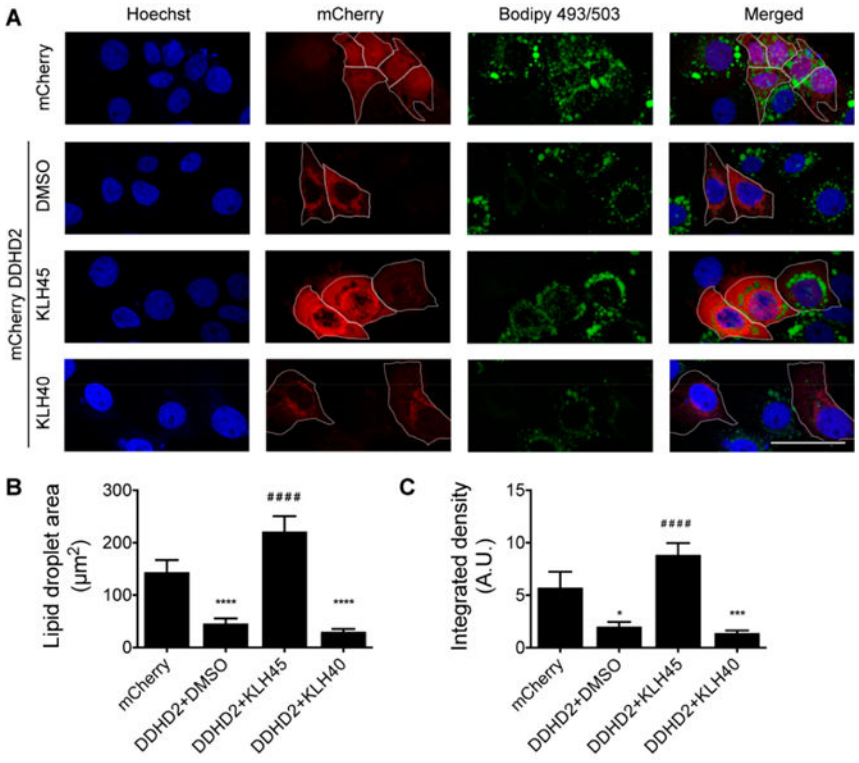

Figure 4.

DDHD2 inhibitor KLH45 increases LD formation in fatty acid-supplemented DDHD2-expressing cells. (A) COS-7 cells transfected with mCherry-DDHD2 were pretreated with KLH45 (2 μM), KLH40 (2 μM), or DMSO for 1 h before being supplemented with C18:1 fatty acid for 16 h. Cells were stained with BODIPY 493/503, and nuclei were labeled with Hoechst. White outlines denote transfected cells as determined by the mCherry signal. The scale bar is 50 μm. (B) Quantification of the LD surface area per transfected cell in each treatment group. (C) Quantification of the BODIPY 493/503 signal intensity per transfected cell in each treatment group. Data represent average values ± SEM of 22–50 cells per group, and results are representative of two independent experiments. *$P < 0.05$, ***$P < 0.001$, and ****$P < 0.0001$ for DDHD2+DMSO or DDHD2+KLH40 vs mCherry control cells. ####$P <$ 0.0001 for DDHD2+KLH45 vs DDHD2+DMSO cells.

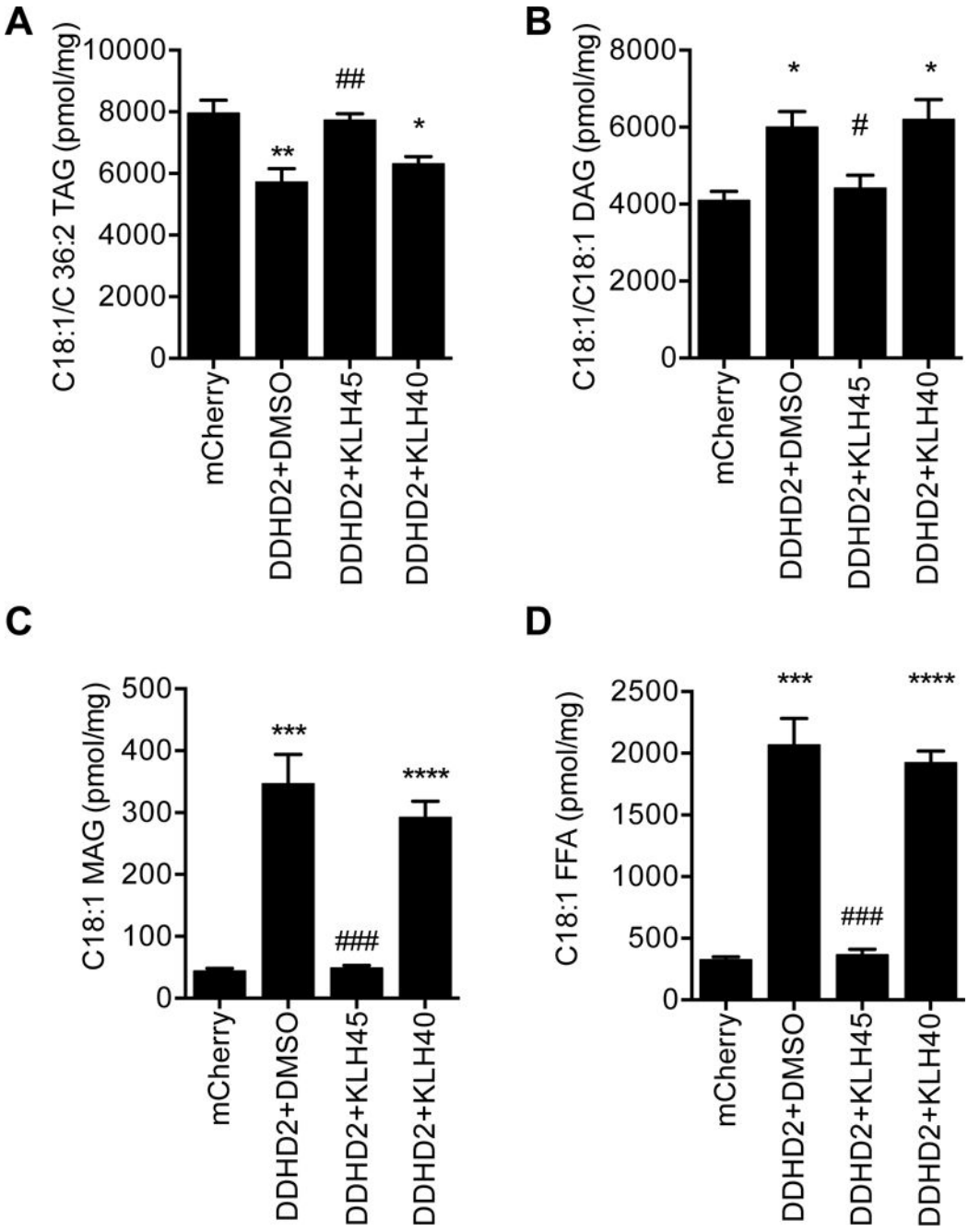

Figure 5.

DDHD2 inhibition restores LD formation in fatty acid-supplemented DDHD2-expressing cells. (A–D) The DDHD2 inhibitor KLH45 (2 μM, 17 h), but not the control inhibitor KLH40 (2 μM, 17 h), blocks C18:1/C36:2 TAG decreases in DDHD2-transfected COS-7 cells supplemented with C18:1 fatty acid (A), as well as elevations in C18:1/C18:1 DAG (B), C18:1 MAG (C), and C18:1 FFA (D). Data represent average values ± SEM ($N = 4$ biological replicates). $^{*}P < 0.05$, $^{**}P < 0.01$, $^{***}P < 0.001$, and $^{****}P < 0.0001$ for DDHD2+DMSO or DDHD2+KLH40 vs mCherry control cells. $\#P < 0.05$, $\#\#P < 0.01$, and $\#\#\#P < 0.001$ for DDHD2+KLH45 vs DDHD2+DMSO cells.

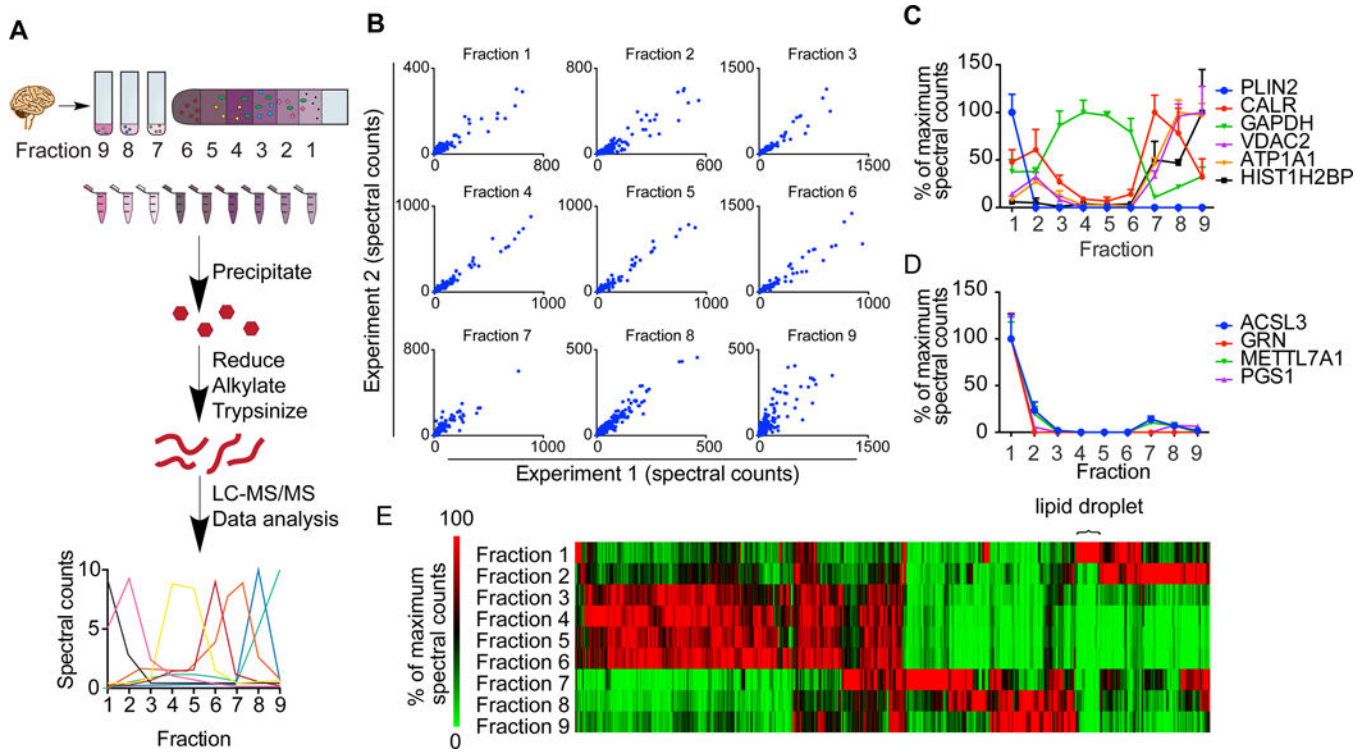

Figure 6.

Protein correlation profiling identifies LD-enriched proteins from brain tissue of DDHD2$^{-/-}$ mice. (A) Schematic representation of the protein correlation profiling experiment. DDHD2$^{-/-}$ mouse brains were homogenized and sequentially fractionated by differential centrifugation and a sucrose density gradient centrifugation. Proteins from all fractions were precipitated and processed in parallel for mass spectrometric analysis. Spectral counts were normalized for each quantified protein across fractions to generate the correlation profiles. (B) Reproducibility of spectral count values for proteins in each fraction from biological replicate experiments. The numbers of spectral counts observed for each protein in experiments 1 and 2 are plotted on the *X*- and *Y*-axes, respectively. Pearson correlation coefficients between all pairwise groups of fractions are reported in Figure S7C. Protein correlation profiles for representative organellar marker proteins: PLIN2, lipid droplets (LDs); CALR, endoplasmic reticulum (ER); GAPDH, cytosol; VDAC2, mitochondria; ATP1A1, plasma membrane; HIST1H2B, nucleus. Data represent average values ± SEM (*N* = 4 biological replicates). (D) Representative LD-enriched proteins in brain tissue from DDHD2$^{-/-}$ mice, defined as proteins with ≥3-fold spectral counts in fraction 1 vs the fraction with the next highest spectral counts that also met the following filtering criteria: ≥15 total spectral counts and detection in fraction 1 in at least three of the four biological replicates. Data represent average values ± SEM (*N* = 4 biological replicates). (E) Hierarchical clustering of proteins based on relatedness of correlation profiles across fractions. Average spectral count values for each protein in each fraction were normalized to the fraction with the most spectral counts for that protein. The horizontal brace highlights the lipid droplet (LD)-enriched cluster that contains 49 members.

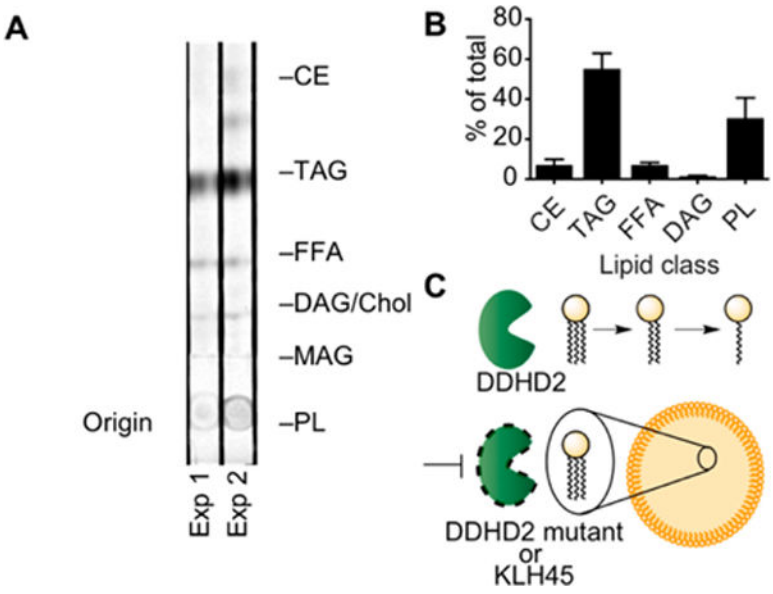

Figure 7.

LDs from brain tissue of DDHD2$^{-/-}$ mice are primarily composed of TAGs. (A) Lipids isolated from the LD fraction from brain tissue of DDHD2$^{-/-}$ mice by a mixture of 4:1:4 (v/v) CHCl3/CH3OH/H2O. Lipid classes were separated by thin layer chromatography (TLC) using an established solvent system[46] and visualized by I_2 staining. Abbreviations: CE, cholesterol ester; TAG, triacylglycerol; FFA, free fatty acids; DAG, diacylglycerol; Chol, cholesterol; MAG, monoacylglycerol; PL, phospholipid. (B) Estimation of relative lipid quantities in the LD fraction as visualized by I_2 staining in panel A. Data respresent average values ± SEM (N = 5). (C) Model to explain how DDHD2 regulates the LD content of neurons. DDHD2 functions as a principal TAG hydrolase in neurons, thereby preventing excessive accumulation of TAGs. Loss of DDHD2, through genetic mutation or chemical inhibition, blocks the metabolism of TAGs, leading to accumulation of TAG-enriched LDs in neurons throughout the CNS.

Table 1

Lipid Droplet (LD)-Associated Proteins Identified in Brain Tissue from DDHD2$^{-/-}$ Mice

UniProt accession number	gene name	lipid droplet GO:0005811	identified as LD-associated in previous proteomic experiments	proteomic references	other references for LD association	hanging justification seems out of place
Q9DBL9	Abhd5	true	yes (5[a])	30–34		Chanarin-Dorfman syndrome (275630)
Q5SWU9	Acaca		yes (4)	30, 32, 33, 35		acetyl-CoA carboxylase 1 deficiency (613933)
Q9CZW4	Acsl3	true	yes (6)	30–33, 36, 37		
Q8K2C8	Agpat6		0		17	
E9Q414	Apob		0			hypercholesterolemia (144010), hypobetalipoproteinemia (615558)
Q9WV54	Asah1		0			spinal muscular atrophy with progressive myoclonic epilepsy (159950), Farber lipogranulomatosis (228000)
Q6P4T0	Atg2a	true	0		38	
P70295	Aup1		yes (2)	30–32		
Q9R171	Cbln1		0			
P61022	Chp1		0			
P18242	Ctsd		yes (1)	31		neuronal ceroid lipofuscinosis (610127)
Q9R013	Ctsf		0			neuronal ceroid lipofuscinosis (615362)
Q99L04	Dhrs1		yes (3)	30, 31, 39		
O88876	Dhrs3		yes (1)	32		
Q6IE26	Ephx4		0			
P70213	Fv1		0			
O70325	Gpx4		0			spondylometaphyseal dysplasia (250220)
P28798	Grn		0			frontotemporal dementia (607485), neuronal ceroid lipofuscinosis (614706)
Q91WA3	Hdac11		0			
Q9EQ06	Hsd17b11	true	yes (5)	30, 33, 37, 39, 40		
O88736	Hsd17b7		yes (5)	30–33, 39		
Q9DCE9	Igtp		yes (1)	31		Crohn’s disease (612278)
Q9JHS3	Lamtor2		0			immunodeficiency (610798)
Q8BVA5	Ldah	true	yes (2)	31, 40		

UniProt accession number	gene name	lipid droplet GO:0005811	identified as LD-associated in previous proteomic experiments	proteomic references	other references for LD association	hanging justification seems out of place
Q8BLN5	Lss	true	yes (6)	31–34, 37, 39, 40		cataract (616509)
Q8C6B0	Mettl7a1	true	yes (4)	30, 31, 36, 40	41	
Q9D7V9	Naaa		0			
Q8BHF7	Pgs1		yes (1)	31		
P43883	Plin2	true	yes (6)	30, 32, 33, 36, 37, 39		
Q9DBG5	Plin3	true	yes (5)	32–34, 37, 40		
O88492	Plin4	true	0		42	
Q8VCH7	Rdh10		0		43	
Q6PDS3	Sarm1		0			
Q8R127	Sccpdh	true	yes (4)	30–32, 37		
O89023	Tpp1		yes (1)	30		neuronal ceroid lipofuscinosis (204500), spinocerebellar ataxia (609270)
Q9DBS2	Tprg1l		0			
Q8R5K2	Usp33		yes (2)	30, 35		
Q8BX70	Vps13c		0			Parkinson’s disease (616840)
Q91VM3	Wdr45		0			neurodegeneration with brain iron accumulation (300894)

[a]Number of proteomic studies in which protein has been identified as LD-associated.